Reproducibility of optical coherence tomography imaging based measurements of the fibrous cap thickness in lipid-enrich atheroma

†Chunliu He[1,2], *Zhiyong Li[1,2,3], Jiaqiu Wang[3], Yuxiang Huang[1,2], Tongjing Zhu[1,2], Yuehong Miao[1,2]

[1] State Key Laboratory of Bioelectronics, Southeast University, Nanjing 210096, P.R. China.

[2]School of Biological Science and Medical Engineering, Southeast University, Nanjing 210096, P.R. China.

3School of Chemistry, Physics and Mechanical Engineering, Queensland University of Technology, Brisbane, QLD 4000, Australia.

† Presenting author: Chunliu He, Southeast University, Nanjing China;

*Corresponding authors: Zhiyong Li, Southeast University, Nanjing China, email: zylicam@gmail.com

Abstract

Rupture of the thin fibrous cap of the atherosclerotic plaque is the primary cause of acute coronary syndrome accounting for more than half of all cardiovascular deaths. Fibrous cap thickness (FCT) is seen as critical to plaque vulnerability. In this study, the intra-observer reproducibility of FCT and the correlation analysis between FCT and intravascular optical coherence tomography (IVOCT) images features were implemented to find the relationship between FCT of lipid-enrich plaques and images information by two observers. We performed IVOCT pullbacks in consecutive series on 20 patients and selected 102 images containing lipid-enrich plaques. Firstly, region of interests (ROIs) were extracted by an unsupervised fuzzy c means clustering (FCM) stage. Then, 32 features, which are associated with the structural and biochemical changes of tissue within the ROIs, were carried out using First order statistics (FOS), Gray level co-occurrence matrix (GLCM), Neighborhood gray tone difference matrix (NGTDM), Invariant moment (IM), Fractal dimension (FD) and Shape features (SF). Finally, the FCT in grayscale IVOCT images were manually measured by two independent observers. The intraclass correlation coefficient (ICC) was 0.80 for two different observers. The image features with ROI region and FCT showed a high correlation coefficient for both observers (r=0.88, p<0.001 and r= 0.91, p<0.001, respectively). The results suggest that the features of IVOCT images based FCT measurements may be useful to quantify the plaque cap thickness and vulnerability.

Keyword: atherosclerotic plaque; intravascular optical coherence tomography; fibrous cap thickness; coronary plaque vulnerability; intra-observer reproducibility

1. Introduction

Coronary atherosclerotic plaque rupture is a major cause of acute coronary syndrome (ACS) [1-3]. Thin-capped fibroatheroma (TCFA) is recognized as a precursor for plaque rupture. The pathologic features of TCFA are a large lipid-enrich necrotic core (the maximum lipid arc>90^o), a thin fibrous cap, and macrophage infiltration into the cap [2-8]. Postmortem studies have shown that a fibrous cap thickness (FCT) (<65um) prone to rupture, the critical threshold was widely accepted [9-11]. The composition and morphology of atherosclerotic plaques are considered to be more important in determining the risk of acute syndromes than the degree of

luminal stenosis [12]. Therefore, detection and quantification of FCT of lipid-enrich atherosclerotic plaque are important for the assessment of plaque vulnerability in order to prevent acute events and monitor interventional treatments.

Intravascular imaging modalities such as intravascular ultrasound (IVUS) and angiography do not have ability to accurately quantify some of the critical components of a vulnerable plaque such as FCT and macrophage content. Intravascular optical coherence tomography (IVOCT), however, is a unique high axial resolution (~10μm) imaging modality capable of characterizing these important morphological features of atherosclerotic plaque. IVOCT has demonstrated its capacity in the identification and quantification of FCT in clinical practice [8, 13, 14].

According to the published consensus standards for IVOCT images, the plaque lipid core is a signal-poor region within an atherosclerotic plaque, with poorly delineated borders, and little or no signal backscattering. In contrast, the fibrous cap has a relatively homogeneous signal with high backscattering. Several semi-automatic and fully-automatic methods have been used to segment lipid and fibrous components by a supervised segmentation based on pixels [15, 16]. The two major drawbacks that hinder such image analysis are: (1) the procedure is cumbersome and time-consuming because of the large number of data points, and (2) manual segmentation as the gold standard are subject to a certain degree of variability between different analysts. Therefore, an unsupervised method based on FCM algorithm was introduced in the study to resolve the poorly delineated borders of the lipid core.

The purpose of this study was to analyze reproducibility of FCT measurements *in vivo*, which were achieved by two independent observers. In addition, we determined the correction coefficient and statistically significant between FCT and IVOCT images features that might mimic lipid-enrich coronary atherosclerosis plaques to assess influence of feature set in quantization FCT.

2. Materials and Methods

2.1 Image dataset

All 33 IVOCT clinical pullbacks of 20 patients were taken from Affiliated Drum Tower Hospital, Nanjing University between December 2015 and December 2016. The IVOCT images were acquired by using a commercially available Fourier Domain OCT (FDOCT) system (2.7F C7-XR, St. Jude Medical, St. Paul, Minnesota) and C7 Dragonfly catheter (St. Jude). The system is equipped with a near-infrared laser light source with a central wavelength of 1310 nm and full-width-at-half-maximum bandwidth of 80 nm. The imaging system provides an axial resolution ~10 um and a lateral resolution of ~30um in biological tissues. Scan parameters were set as 100 frames/sec, 54,000 A-scans/sec, pullback speed of 20 mm/sec, pullback length of ~54.2 mm. This study was approved by the institutional human ethics committee. All the patients have given explicitly informed consent. IVOCT images including lipid-enrich plaques from all pullbacks were selected from all databases. Out of these images, only segments containing lipid-enrich plaques were selected based on the published consensus standards [5] and the improvement of standard interpretation algorithm [17]. Total of 102 images were selected for analysis.

2.2 Manual measurement fibrous cap thickness

Measurement FCT of atherosclerotic plaques is difficult because of its complex structures with discrete individual components, especially lipid-enrich plaque with seriously diffuse border. Therefore, observers of measurement were familiar with related work and had a deep knowledge of American College of Cardiology clinical expert consensus document on standards. 102 images were analyzed by two expert observers using an OCT system software (LightLab Imaging Inc., Westford, Massachusetts). The representative FCT measurements of IVOCT images in lipid-enrich plaque from two observers is shown in Figure 1. For each plaque, both observers selected the same images from the IVOCT run and measured the thinnest FCT two times, from which the final measurement value of FCT was calculated by averaging.

Observer 1 Observer 2

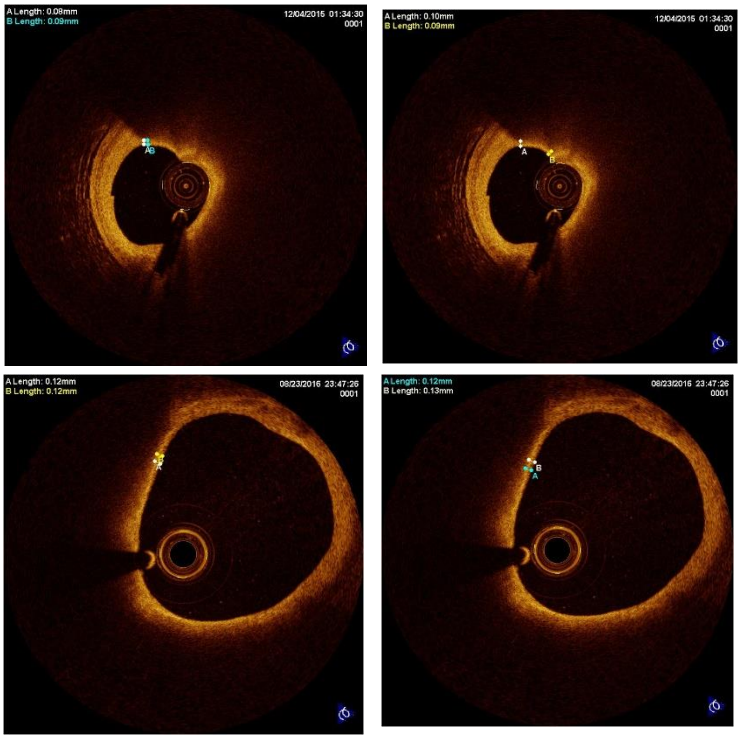

Figure 1. The representative IVOCT images for measurements of FCT by observer 1 and observer 2

3. Image Analysis

3.1 Pre-processing

Consider the IVOCT images in polar coordinates (θ, r) where θ is angle and r is depth. $I(i, j)$ represents intensity of each pixel at row i and column j. Ring-area (RA) and Lumen are automatically segmented by processing the following four steps. The results of each step are shown in Figure 2.

1. Remove guide-wire and artifacts;

$$I\left(:,1:\underset{1\le j\le n}{max}\left(\bar{I}(i,j)\right)+wc\right)=0 \quad (1)$$

$$I\left(\underset{1\le i\le m}{min}\left(\bar{I}(i,j)\right)\pm wr,:\right)=0 \quad (2)$$

where $\bar{I}(i,j)$ refers to the average of pixel value, and wc and wr are the thresholds. The parameter values $wc=50$ and $wr=10$ used in the paper were determined based on catheter size.

2. Binarization images processed by adaptive threshold OSTU's method algorithm and by morphological connect neighborhood and area constraint [18];
3. Lumen was automatically segmented by connecting the nonzero pixels, interpolating pixels of full zero row, and then expanding lumen to 1mm to take into account the limited penetration depth of OCT system;
4. The polar images were subsequently converted to a cartesian coordinate in order to reconstruct an image that preserved the true morphology of visualization.

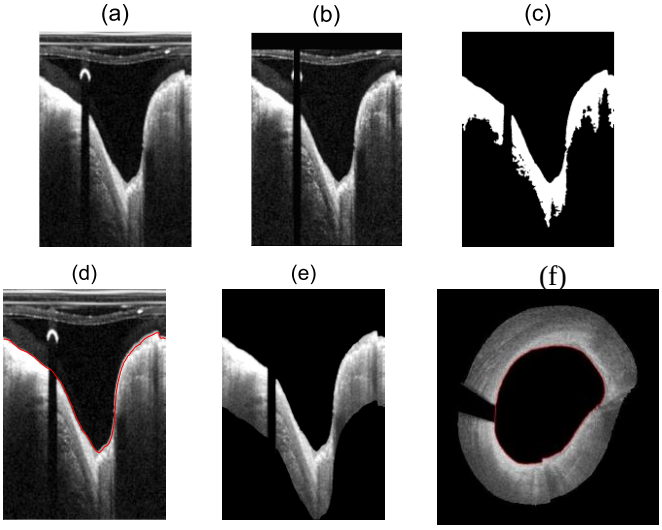

Figure 2. Illustration of the using fully-automated segmentation procedure. Image (a) shows original raw polar domain image; Image (b) show the guide-wire and catheter artifacts remove result partially; Image (c) illustrates the application of the Otsu's method, morphological operations and the area constrain; Image (d) shows lumen segmentation result; Image (e) and (f) show the RA segmentation results before and after scan-conversion respectively.

3.2 Region of interest (ROI) extraction

Compared to fibrous cap, necrotic lipid core exhibits a lower signal density and a more heterogeneous back-scattering [19, 20]. Lipid core area has the following major characteristics: diffusely bordered, signal-poor regions with overlying signal-rich bands. In this paper, FCM method was selected to extract the cap of fibrous components [21]. Once the cap of fibrous components was segmented, the lipid core borders were subsequently obtained by arc angle of lumen contours. In the paper, the research problem with the green contour model were formulated as shown in Figure 3(a). The contour of a cap of fibrous component in the 2-D image was represented by two curves along *x-axis* and y-*axis* in Figure 3 (b) and (c). A simple polynomial curve fitting algorithm was proposed in order to smooth two curves. Next, the key

problem was to locate the two points pointed by the white arrow to extract ROI. We used the simple geometric constraints: the catheter center set as an origin, four equal regions were divided, the same arc angle in Figure 3 (b) and (c) are the points indicated by white arrow in Figure 3 (a). Figure 4 gives three representative results of the ROI in different pullbacks.

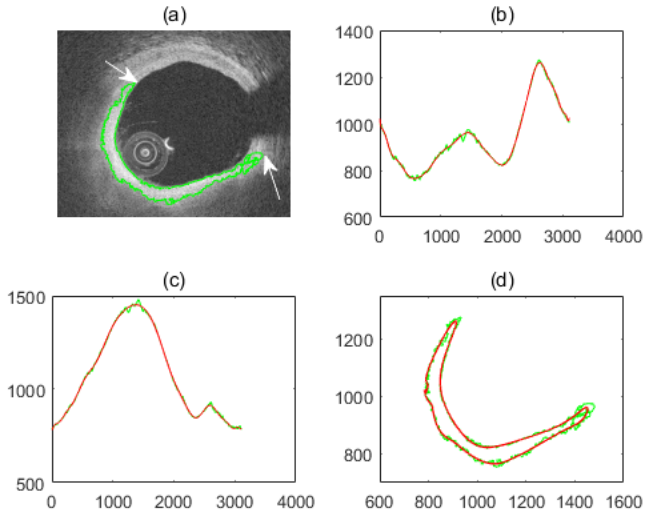

Figure 3. The cap of fibrous component extraction algorithm using the FCM combination with geometric constraint. The green contour of image (a) shows the cap segmentation result based on the FCM algorithm. Image (b) and (c) display the fitting results using polynomial curve fitting algorithm. The green line and red line represent the row and column index value before and after polynomial curve fitting, respectively. Image (d) shows the cap contours before and after polynomial curve fitting.

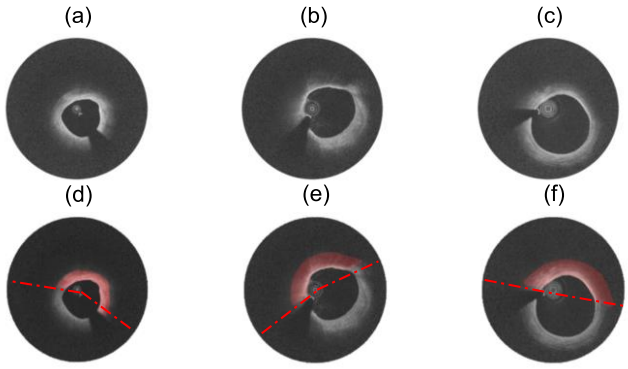

Figure 4. Representative results of the ROI on three frames from different pullbacks. Image (a), (b) and (c) show the log image with lipid-enrich plaques in the cartesian coordinate. Image (c), (d) and (f) show the ROIs (red regions) corresponding to the image (a), (b) and (c), respectively.

3.3 Feature extraction

Texture features and shape parameters were extracted from ROIs. Texture refers to the spatial interrelationship and arrangement of the basic elements of an image [22, 23]. Texture features have to be derived from the gray images because the spatial interrelationships and the arrangements of the image pixels are seen as variations in the intensity patterns or gray tones visually. Although it is easy for humans to recognize different kinds of textures, it is quite a

difficult task to define and interpret the textures automatically by computer algorithm. Shape is also an important feature for medical image [12]. In this paper, six different feature sets composing of a total 32 features were listed in table 1. The implementation details for the texture feature and shape parameters and referred papers are shown below:

Table 1. Feature sets information and corresponding references.

Feature sets	Feature name	Reference
FOS	mean, variance, median, skewness, kurtosis	[23]
GLCM	correlation, contract, dissimilarity, energy, entropy, homogeneity, maximum probability.	[24]
NGTDM	busyness, contrast, complexity, coarseness, texture length	[25]
IM	I1,I2,I3,I4,I5,I6,I7	[26]
FDTA	H^1 , H^2 , H^3 , H^4	[23] [27]
SP	eccentricity, perimeter, majoraxislength (mal), minoraxislength (mil)	[23]

3.4 Statistical analysis

Inter-observer agreement and intra-observer reproducibility estimates were analyzed using the two paired t-test, intraclass correlation coefficient (ICC), and Bland Altman analyses estimating 95% limits of agreement (LOA). LOA was defined as mean 1.96±SD of absolute difference by Bland–Altman method. Generally, an ICC <0.4, between 0.4-0.75, and >0.75 indicates poor, moderate, and excellent agreement, respectively [28]. Initially, univariate linear regressions were performed between each thickness measure and IVOCT image features. Direct linear regression was appropriate here, because the IVOCT images sampling interval was far more than 0.2 mm and the data at nearby points were independent. In addition, for each of the 102 thickness measures, multivariate linear regressions were performed against all 32 image features. Multiple correlation coefficient between variables was estimated using Pearson's correlation coefficient (r). For all test, a two tailed p value<0.05 was considered statistically significant. All statistical analysis was performed with SPSS statistical software (IBM SPSS Statistics for Windows, Version 19.0. IBM Corp., Armonk, New York).

4. Result

The ICCs (0.99 for observer 1 and 0.99 for observer 2) of FCT measurement showed excellent agreement and reproducibility (ICC=0.80 between observer 1 and 2). FCT11, FCT12 represented two measurement results by observer 1, FCT21, FCT22 were the measurement results by observer 2, mFCT1 and mFCT2 were the mean by observer 1 and 2. The Bland–Altman plots showed LOAs of different FCT measurements from two observers (Figure 5). The LOAs for FCT11 vs FCT21, FCT11 vs FCT22, FCT12 vs FCT21 and FCT12 vs FCT22 were 110, -55um (p=0.016), 130, -43um (p=0.03), 100, -66um (p=0.008) and 110, -53um (p=0.015), respectively.

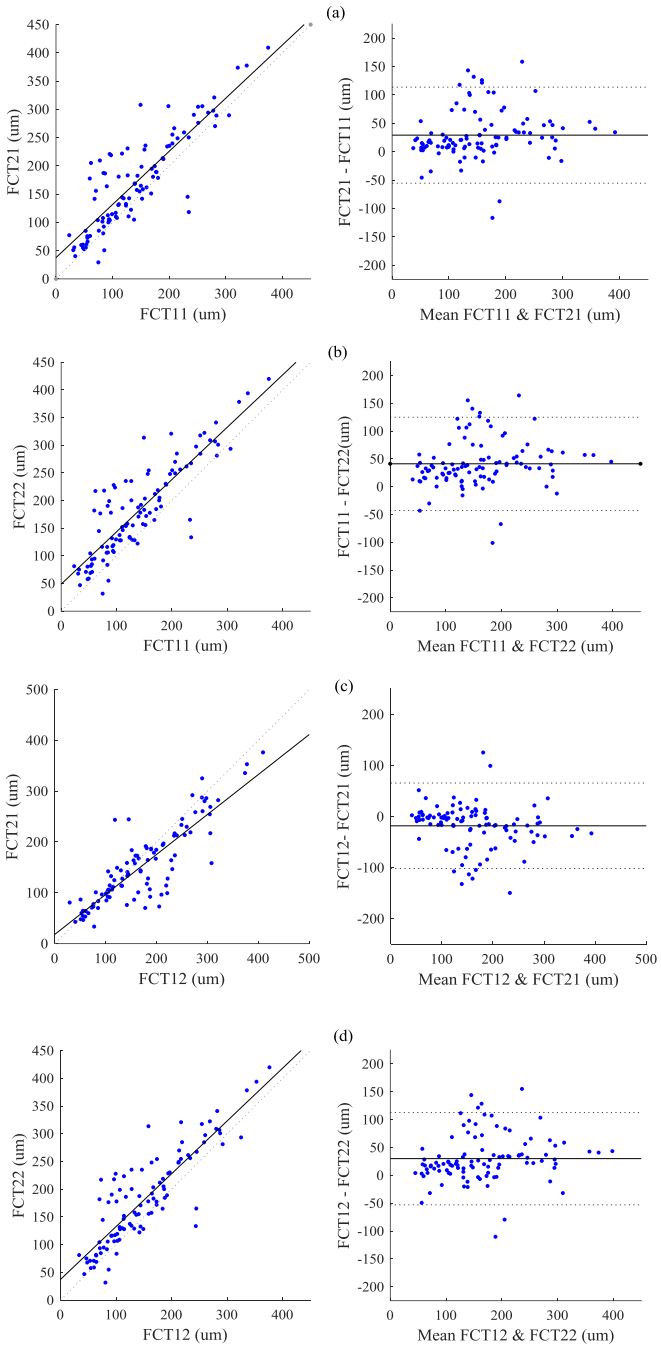

Figure 5. Comparison of the FCT measured by observer 1 versus observer 2 (left panels) Bland-Altman test for two observers in measurement of FCT (right panels).

Table 2. The correction coefficient of mFCT and univariate image features by two observers

	mFCT1		mFCT2			mFCT1		mFCT2	
feature name	*r*	*p*-value	*r*	*p*-value		*r*	*p*-value	*r*	*p*-value
mean	0.62	<0.001	0.64	<0.001	texture length	0.39	<0.001	0.38	<0.001
variance	0.48	<0.001	0.49	<0.001	I1	0.53	<0.001	0.54	<0.001
median	0.45	<0.001	0.48	<0.001	I2	0.13	**0.1848**	0.22	0.03
skewness	0.48	<0.001	0.51	<0.001	I3	0.33	<0.001	0.33	<0.001
kurtosis	0.52	<0.001	0.53	<0.001	I4	0.03	**0.73**	0.05	**0.59**
correlation	0.59	<0.001	0.61	<0.001	I5	0.01	**0.97**	0.13	**0.19**
contract	0.58	<0.001	0.61	<0.001	I6	0.36	<0.001	0.28	<0.001
dissimilarity	0.59	<0.001	0.62	<0.001	I7	0.47	<0.001	0.50	<0.001
energy	0.60	<0.001	0.64	<0.001	H^1	0.16	**0.12**	0.08	**0.43**
entropy	0.49	<0.001	0.48	<0.001	H^2	0.16	**0.12**	0.08	**0.41**
homogeneity	0.33	<0.001	0.35	<0.001	H^3	0.45	<0.001	0.44	<0.001
maximum probability	0.34	<0.001	0.34	<0.001	H^4	0.01	**0.95**	0.06	**0.56**
busyness	0.23	0.01	0.25	0.0112	eccentricity	0.17	**0.09**	0.27	<0.001
contrast	0.37	<0.001	0.36	<0.001	perimeter	0.08	**0.42**	0.16	**0.10**
complexity	0.06	**0.52**	0.16	**0.1**	mal	0.16	**0.11**	0.26	0.01
coarseness	0.39	<0.001	0.39	<0.001	mil	0.30	0.0021	0.41	<0.001

Table 2 reports statistically significant (*p*) and Pearson correction coefficient (*r*) between univariate feature and mFCT. The correction coefficient is generally low, where the lowest and highest values are 0.62 (mean) and 0.01 (I5 and H^4) from observer 1 and 0.64 (mean and energy) and 0.05 (I4) from observer 2. Bold *p*-values represent no statistically significant between two

variable values.

Similarly, Table 3 shows statistically significant (*p*) and Pearson correction coefficient (*r*) between multivariate feature sets and mFCT. Statistically significant results were observed in both two groups i.e. individual group feature set and the fusion feature set. The lowest correction coefficient of individual group appeared at shape parameter group (feature set 6), which were 0.48 and 0.58 for observer 1 and 2, respectively. The phenomenon was in turn confirmed in Table 2 that the correction coefficient of four shape parameters were overall lower than others. In the contrast, the highest correction coefficient of individual group was observed in feature set 2, which were 0.78 and 0.80, respectively. For both groups, Pearson correlation coefficient of the fusion feature sets for observers 1 and 2 were 0.88 and 0.91, which better than any individual group feature set.

Table 3. The correction coefficient of mFCT and multivariate image features by two observers

Feature set	mFCT1		mFCT2	
	r	*p*-value	*r*	*p*-value
FOS	0.67	<0.001	0.68	<0.001
GLCM	0.78	<0.001	0.80	<0.001
NGTDM	0.68	<0.001	0.74	<0.001
FD	0.74	<0.001	0.72	<0.001
IM	0.52	<0.001	0.62	<0.001
SP	0.48	<0.001	0.58	<0.001
Fusion feature sets	0.88	<0.001	0.91	<0.001

5. Discussion

It is an important role of FCT as indicators of vulnerable plaques which could potentially guide appropriate surgical treatment such as percutaneous coronary intervention (e.g., balloon angioplasty or stent placement). Therefore, there is a strong desire to treat these lesions before they cause harm. The reliable examination of these indicators of atherosclerotic plaques will ultimately determine the clinical value of IVOCT, depending on the application of meaningful and reproducible methods. The main findings of the present study are the excellent inter-observer agreement of the manual assessment of FCT and excellent intra-observer reproducibility in the FCT measurement. In addition, the high correction between the feature of ROIs and mFCT measured by two observers, which show that IVOCT image feature is able to provide more information in quantization FCT to promote both the computer-aided routine clinical use and analysis of large-scale data sets from clinical trials in vulnerable plaque.

The current accepted universal method for assessing FCT *in vivo* using IVOCT images is based on single measurement of the thinnest portion of the fibrous cap [14, 29]. In practice, the extensive clinical image data *in vivo* were usually analyzed manually by expert analysts. Indeed, the excellent inter-observer agreement of IVOCT images to measure the FCT manually, have been previously reported. Kim et al. [30] performed first *in vivo* investigation in the inter-observer agreement (ICC=0.99) and intra-observer reproducibility (ICC=0.49) of FCT by 4 independent observers. Subsequently, Gerbaud et al [31] reported intra-observer reproducibility

of FCT was moderate (ICC=0.48). In the present study, excellent inter-observer agreement resulted for FCT measurement, with ICC of 0.99 was reached in the analysis and was similar to literature previously. Greatly, excellent intra-observer reproducibility (ICC=0.80) was achieved for FCT measurement, higher than the result of the previous mentioned studies. Recently, Kini et al [17] studied intra-observer reproducibility before and after developing the lesion assessment criteria with 170 pullbacks. The result shown that a significantly higher level for FCT measurement, with ICC of 0.82 compared with the observed in our study of reproducibility *in vivo* measurement. However, these independent observers extensively learned the development of standard interpretation criteria formulated which significantly provided the level of intra-observer reproducibility. The lower intra-observer reproducibility in our study may, in part, be explained by the heterogeneity in the coronary plaques imaged. Indeed, the patients in our study are more likely to have lipid-enrich, complex plaques, with a higher potential for intra-observer variability. Although learning the standard interpretation algorithm, a limited pullback data may cause a low learning outcomes result. Therefore, more data are more likely to represent a true reproducibility value, based on the current commercial available IVOCT systems.

Although others' and our studies had been certified the FCT measurement may be repeatable by independent observer manually, few literates focus on the interrelationship between IVOCT image feature information and FCT. Such an idea will help in enhancing the significance of noninvasive coronary artery tests in the identification of FCT and assessment the risk factors of stroke. Thus, in the study, we first analyzed the correct coefficient and statistically significant between FCT and the six group image features based on the priori knowledge that the more higher the correction coefficient, the better elucidate the texture feature was used to quantify FCT.

The results in this study (Table 2 and Table 3) indicate significant relationships between feature sets and FCT. The *r* value of the univariate regressions indicate that only several single texture feature factor are dominant in determining FCT, there are mean, contract, dissimilarity, energy, entropy, homogeneity, maximum probability (Table 2). On the other hand, the individual feature set of the multivariate regressions are all highly significant, and the correlation coefficients are substantially higher as well (Table 3). Thus, thickening seems to be influenced by multiple aspects of the texture feature and shape parameters. This is to be expected, the texture features are postulated to act through their influence on the spatial interrelationships and arrangement of the gray image, and it is reasonable that each of these FCT (the minimum distance implied in the spatial arrangement) would be influenced by texture feature and shape parameters. Best feature sets were the GLCM feature set, followed by the FDTA. In general, all individual feature set performed in a range of about 0.52-0.78 and 0.62-0.80 for observer 1 and 2, except of the shape parameters that performed much worse. In order to enhance the influences of feature set, the six feature sets were combined, by connecting the feature one by one. Fusing results of the six different feature sets, improved the correction results obtained by the individual feature sets, reaching an average correction coefficient of 0.88 and 0.91 for the observer 1 and 2. The benefits of fusion results are more obvious in the case where there is no dominant best feature sets, as the case with the features extracted from the lipid-enrich plaque images in this study. It

is noteworthy in this respect that the signs of the regression coefficients in the univariate and multivariate regressions in Tables 2 and 3 are consistent.

Study Limitations

In multivariate regression analysis, correlation among the independent variables is one common problem. The problem may be an influential factor if the primary purpose of the regression is to identify important explanatory variables that might play a causal role. The estimated regression coefficients for such correlated variables can be different. This problem was not involved and discussed in our case. Feature selection method with deleting the possible correlations between the independent variables are suggested in the future research.
In computer vison analysis, efficiency measured by the computational time is another common problem. Computational times for preprocessing, lumen segmentation, scan-conversion and ROI extraction were recorded by matlab code, especially scan-conversion spent a long time (two hours for 271 images) in the study. As such, further coding and implementation in a faster language (e.g. C/C++) would significantly reduce computational time, possibly achieving the analysis of a multiple IVOCT images in a time a few minutes.

Lack of histology data as the golden standard in the FCT measurement is the third problem. Given that IVOCT manual FCT measurement of atherosclerotic plaques is subject to some inter-observer variability, the use of a third reader is always required in case of disagreement between two readers. As a matter of fact, only FCT measurement using a large series of histological samples would be able to give more objective and detailed results. However, even if histology can provide a stronger ground truth, the correct registration with IVOCT images can be a challenge due to histological slice thickness and helicoidal IVOCT data acquisition [32, 33]. Therefore, a large amount of histological data would be required to achieve enough statistical analysis result, which is not currently available.

Conclusion

We discussed the variabilities between observers for quantifying the FCT in human coronary arteries based on IVOCT using manual measurement. Intra-reproducibility result demonstrate that FCT was repeated by manual measurements in lipid-enrich atherosclerotic plaque. In addition, we analyzed the relationship between FCT and image feature. The regression result demonstrated the fusion feature played an important role in quantification FCT for online identification of high-risk plaques.

References

[1] Yonetsu T, Kakuta T, Lee T, Takahashi K, Kawaguchi N, Yamamoto G, et al. In vivo critical fibrous cap thickness for rupture-prone coronary plaques assessed by optical coherence tomography. *European Heart Journal* 2011; 32(10): 1251-1259.

[2] Habara M, Nasu K, Terashima M, Ko EH, Yokota D, Ito T, et al. Impact on optical coherence tomographic coronary findings of fluvastatin alone versus fluvastatin plus ezetimibe. *American Journal of Cardiology* 2014; 113(4): 580-587.

[3] Cardoso L, Weinbaum S. Changing views of the biomechanics of vulnerable plaque rupture: a review. *Annals of Biomedical Engineering* 2014; 42(2): 415-431.

[4] Di Vito L, Yoon JH, Kato K, Yonetsu T, Vergallo R, et al. Comprehensive overview of definitions for optical coherence tomography-based plaque and stent analyses. *Coronary Artery Disease* 2014; 25(2): 172-185.

[5] Falk E, Nakano M, Bentzon JF, Finn AV, Virmani R. Update on acute coronary syndromes: the pathologists' view. *European Heart Journal* 2013; 34(10): 719-746.

[6] Fujii K, Hao H, Shibuya M, Imanaka T, Fukunaga M, Miki K, et al. Accuracy of OCT, grayscale IVUS, and their combination for the diagnosis of coronary TCFA: an ex vivo validation study. *JACC: Cardiovasc Imaging* 2015; 8(4): 451-460.

[7] Jang IK, Tearney GJ, MacNeill B, Takano M, Moselewski F, Iftima N, et al. In vivo characterization of coronary atherosclerotic plaque by use of optical coherence tomography. *Circulation* 2005; 111(12): 1551-1555.

[8] Virmani R, Burke AP, Farb A, Kolodgie FD. Pathology of the vulnerable plaque. *Journal of the American College of Cardiology* 2006; 47(8 Suppl): 13-18.

[9] Tanaka A, Imanishi T, Kitabata H, Kubo T, Takarada S, Tanimoto T, et al. Lipid-rich plaque and myocardial perfusion after successful stenting in patients with non-ST-segment elevation acute coronary syndrome: an optical coherence tomography study. *European Heart Journal* 2009; 30(11): 1348-1355.

[10] Tearney GJ, Jang IK, Bouma BE. Optical coherence tomography for imaging the vulnerable plaque. *Journal of Biomedical Opticst* 2006; 11(2): 021002.

[11] Tian J, Dauerman H, Toma C, Samady H, Itoh T, et al. Prevalence and characteristics of TCFA and degree of coronary artery stenosis: an OCT, IVUS, and angiographic study. *Journal of the American College of Cardiology* 2014; 64(7): 672-680.

[12] Wang Z, Liu N, Zhang L, Li X, Han X, Peng Y, et al. Real-time elastography visualization and histopathological characterization of rabbit atherosclerotic carotid arteries. *Ultrasound in Medicine and Biology* 2016; 42(1): 176-184.

[13] Jang IK, Bouma BE, Kang DH, Park SJ, Park SW, Seung KB, et al. Visualization of coronary atherosclerotic plaques in patients using optical coherence tomography: comparison with intravascular ultrasound. *Journal of the American College of Cardiology* 2002; 39(4): 604-609.

[14] Kubo T, Imanishi T, Takarada S, Kuroi A, Ueno S, Yamano T, et al. Assessment of culprit lesion morphology in acute myocardial infarction: ability of optical coherence tomography compared with intravascular ultrasound and coronary angioscopy. *Journal of the American College of Cardiology* 2007; 50(10): 933-939.

[15] Wang Z, Chamie D, Bezerra HG, Yamamoto H, Kanovsky J, Wilson DL, et al. Volumetric quantification of fibrous caps using intravascular optical coherence tomography. *Biomedical Optics Express* 2012; 3(6): 1413-1426.

[16] Athanasiou L S, Bourantas C V, Rigas G, et al. Methodology for fully automated segmentation and plaque characterization in intracoronary optical coherence tomography images. *Journal of Biomedical Opticst*, 2014, 19(2): 026009.

[17] Kini AS, Vengrenyuk Y, Yoshimura T, Matsumura M, Pena J, Baber U, et al. Fibrous cap thickness by optical coherence tomography in vivo. *Journal of the American College of Cardiology* 2017; 69(6): 644-657.

[18] Koga S, Ikeda S, Yoshida T, Nakata T, Takeno M, Masuda N, et al. Elevated levels of systemic pentraxin 3 are associated with thin-cap fibroatheroma in coronary culprit lesions assessment by optical coherence tomography and intravascular ultrasound. *JACC: Cardiovascular Interventions* 2013; 6(9): 945-954.

[19] Prati F, Guagliumi G, Mintz GS, Costa M, Regar E, Akasaka T, et al. Expert review document part 2: methodology, terminology and clinical applications of optical coherence tomography for the assessment of interventional procedures. *European Heart Journal* 2012; 33(20): 2513-2520.

[20] Prati F, Regar E, Mintz GS, Arbustini E, Di Mario C, Jang IK, et al. Expert review document on methodology, terminology, and clinical applications of optical coherence tomography: physical principles, methodology of

image acquisition, and clinical application for assessment of coronary arteries and atherosclerosis. *European Heart Journal* 2010; 31(4): 401-415.

[21] Chamie D, Bezerra HG, Attizzani GF, Yamamoto H, Kanaya T, Stefano GT, et al. Incidence, predictors, morphological characteristics, and clinical outcomes of stent edge dissections detected by optical coherence tomography. *JACC: Cardiovascular Interventions* 2013; 6(8): 800-813.

[22] Kato K, Yonetsu T, Jia HB, Abtahian F, Vergallo R, Hu SN, et al. Nonculprit coronary plaque characteristics of chronic kidney disease. *Circulation:Cardiovascular Imaging* 2013; 6(3): 448-471.

[23] Christodoulou CI, Pattichis CS, Pantziaris M, Nicolaides A. Texture-based classification of atherosclerotic carotid plaques. *IEEE Transactions on Medical Imaging* 2003; 22(7): 902-912.

[24] Kalyan K, Jakhia B, Lele RD, Joshi M, Chowdhary A. Artificial neural network application in the diagnosis of disease conditions with liver ultrasound images. *Advances in Bioinformatics* 2014; 708279.

[25] Araki T, Ikeda N, Shukla D, Jain PK, Londhe ND, Shrivastava VK, et al. PCA-based polling strategy in machine learning framework for coronary artery disease risk assessment in intravascular ultrasound: a link between carotid and coronary grayscale plaque morphology. *Computer Methods and Programs in Biomedicine* 2016; 128: 137-158.

[26] Yoshikawa D, Ishii H, Kurebayashi N, Sato B, Hayakawa S, Ando H, et al. Association of cardiorespiratory fitness with characteristics of coronary plaque: Assessment using integrated backscatter intravascular ultrasound and optical coherence tomography. *International Journal of Cardiology* 2013; 162(2): 123-128.

[27] Qiu WB, Chen Y, Li X, Yu YY, Cheng WF, Tsang FK, et al. An open system for intravascular ultrasound imaging. *IEEE Transactions on Ultrasonics Ferroelectrics and Frequency Control* 2012; 59(10): 2201-2209.

[28] Radu MD, Yamaji K, Garcia-Garcia HM, Zaugg S, Taniwaki M, Koskinas KC, et al. Variability in the measurement of minimum fibrous cap thickness and reproducibility of fibroatheroma classification by optical coherence tomography using manual versus semi-automatic assessment. *EuroIntervention* 2016; 12(8): 987-997.

[29] Kume T, Akasaka T, Kawamoto T, Okura H, Watanabe N, Toyota E, et al. Measurement of the thickness of the fibrous cap by optical coherence tomography. *American Heart Journal* 2006; 152(4).

[30] Kim SJ, Lee H, Kato K, Yonetsu T, Xing, L, Zhang S, and Jang IK. Reproducibility of in vivo measurements for fibrous cap thickness and lipid arc by OCT. *JACC: Cardiovascular Imaging* 2012, 5(10): 1072-1074.

[31] Gerbaud E, Weisz G, Tanaka A, Kashiwagi M, Shimizu, Wang L, et al. Multi-laboratory inter-institute reproducibility study of IVOCT and IVUS assessments using published consensus document definitions. *European Heart Journal Cardiovascular Imaging* 2016, 17(7):756-764.

[32] Rieber J, Meissner OG, Babaryka S, Reim M, Oswald A, Koenig TM et al. Diagnostic accuracy of optical coherence tomography and intravascular ultrasound for the detection and characterization of atherosclerotic plaque composition in ex-vivo coronary specimens: a comparison with histology *Coronary Artery Disease* 2006, 17(5): 425–430.

[33] Meissner OA, Rieber J, Babaryka G, Oswald M, Reim S, Siebert U, Redel T et al. Mueller- Lisse U., Intravascular optical coherence tomography: comparison with histopathology in atherosclerotic peripheral artery specimens, *Journal of vascular & interventional radiology* 2006, 17(2): 343–349.